ORIGINAL PAPER

Mobile ion transport pathways in $(LiBr)_x[(Li_2O)_{0.6}(P_2O_5)_{0.4}]_{(1-x)}$ glasses

Tho Thieu Duc · Prasada Rao Rayavarapu · Stefan Adams

Abstract $(LiBr)_x[(Li_2O)_{0.6}(P_2O_5)_{0.4}]_{(1-x)}$ glasses with $0 \leq x \leq 0.2$ are prepared by melt quenching. Glass transition temperature (T_g), ionic conductivity (σ), and its activation energy (E_a) are determined experimentally and correlated to molecular dynamics (MD) simulations with an optimized potential, fitted to match bond lengths, coordination numbers, and ionic conductivity. Based on equilibrated MD configurations, ion transport pathways are modelled in detail by the bond valence approach to clarify the influence of the halide dopant concentration on the glass structure and its consequence for Li ion mobility. Results of experimental and computational studies are compared with our previous report on the $(LiCl)_x[(Li_2O)_{0.6}(P_2O_5)_{0.4}]_{(1-x)}$ system. Both T_g and σ values are higher for LiBr-doped glasses than for LiCl-doped glasses, but the effect of halide doping is unusually small.

Keywords Molecular dynamics · Lithium ion conduction · Bond valence · Ion transport in glasses

Introduction

Glasses with fast Lithium ion conduction are widely studied for their potential applications in electrochemical devices. However, the mechanism of ionic conductivity in these materials and in particular the effect of halide dopants is yet to be understood in detail. The glass-forming region in the

T. Thieu Duc · P. R. Rayavarapu (✉) · S. Adams
Department of Materials Science and Engineering,
National University of Singapore,
Singapore 117574, Singapore
e-mail: mserpr@nus.edu.sg

ternary glass system $LiPO_3$–LiX [X=I, Br, Cl] has been reported along with their ionic conductivity (σ) [1], but structures of LiBr-doped lithium phosphate glasses have not yet been studied in the literature, whereas the structures of binary phosphate glasses have been clarified by neutron and X-ray diffraction [2–4], MD simulations [5–10], and spectroscopic techniques [11].

Lithium phosphate binary glasses can be prepared up to 67 mol.% Li_2O. Glasses form up to 30 mol.% LiCl or 33 mol.% LiBr and LiI; σ increases with halogen ion size (and polarizability) and with the increase of LiX content throughout the glass-forming region [1]. Most reports on ternary glass systems deal with LiCl-doped glasses [11–15]. For all Li_2O/P_2O_5 ratios studied, the glass transition temperature T_g decreases and σ increases as the LiCl content increases. The addition of the network modifier Li_2O breaks up P–O–P bridges, creating non-bridging oxygens (NBOs) that reduce the phosphate chain lengths. The addition of the dopant LiCl does not bring about any such modification of chain, though it reduces the T_g of the parent glass [16]. X-ray diffraction and MD simulations of $(LiCl)_x[(Li_2O)_{0.6}(P_2O_5)_{0.4}]_{(1-x)}$ (x=0,0.13,0.25) glasses [14, 15] demonstrate that the addition of Li_2O breaks up the 3D branched phosphate structure, and the addition of LiCl reduces the rigidity and widens channels for Li^+ movement, thus enhancing σ and decreasing T_g. Further structural reports for Li_2O–P_2O_5–LiCl glass [9, 15] confirm that no P–Cl bonds are formed and that LiCl dissolves "interstitially" in the $LiPO_3$ glass network. In line with these findings, none of the six known complex oxyhalide crystal structures that contain P^{5+} shows a bond between phosphorous and the halide ion. In $Li_4X(BePO_4)_3$ with X=Cl or Br, the halide ion is bonded exclusively to Li; in LiF-metal phosphates, the second metal (Al, Ni, V) forms bonds with the F^- ions, but phosphorous is again coordinated by

Table 1 Results of composition analysis of $(LiBr)_x[(Li_2O)_{0.6}(P_2O_5)_{0.4}]_{(1-x)}$ glass

Nominal Composition (mol%)	Theoretical $wt_{Br\%}$	Experimental $wt_{Br\%}$	Experimental glass composition (mol%)
$(Li_2O)_{0.54}(P_2O_5)_{0.36}(LiBr)_{0.10}$	10.52	10.1(7)	$(Li_2O)_{0.54}(P_2O_5)_{0.36}(LiBr)_{0.096}$
$(Li_2O)_{0.51}(P_2O_5)_{0.34}(LiBr)_{0.15}$	15.66	15.6(4)	$(Li_2O)_{0.51}(P_2O_5)_{0.34}(LiBr)_{0.15}$
$(Li_2O)_{0.48}(P_2O_5)_{0.32}(LiBr)_{0.20}$	20.72	20.5(6)	$(Li_2O)_{0.48}(P_2O_5)_{0.32}(LiBr)_{0.199}$

oxygen only. In all these structures, Li^+ have mixed oxyhalide coordination. IR and XPS studies of $(2LiCl)_x(Li_2O)_y(P_2O_5)_{(100-x-y)}$ [$x=0$, 10, 20, $y=50$, 60] are, however, interpreted by Horiuchi et al. [13] as signs that the open halide-doped glass structure is achieved by Cl^- altering the P–O–P network.

While Raman, IR spectroscopy, and Reverse Monte Carlo fits of diffraction data accordingly find that LiCl acts as a dopant in lithium borate glasses [17, 18], the addition of LiCl in Li_2O–TeO_2–LiCl glasses [19, 20] is reported to produce NBOs and hence also Te–Cl bonds. ^7Li MAS NMR studies of $LiCl$–Li_2O–P_2O_3 suggest the existence of LiCl aggregates for high LiCl contents close to the limit of the glass forming region, and it is concluded that these contribute to the high mobility of Li^+ ion [21]. Yet, another impedance spectroscopy study of Li_2X–B_2O_3–SiO_2 ($X=O$, Cl_2) [22] concludes that Cl^- doping acts via modifying the B–O bond strengths and that the network dilatation would be of influence for Li^+ ion conductivity. In sharp contrast, we recently demonstrated the relation between pathway volume of mobile Li^+ ion and the influence of LiCl content in $(LiCl)_x[(Li_2O)_{0.6}(P_2O_5)_{0.4}]_{(1-x)}$ glasses (with $0.1 \leq x \leq 0.25$) and could rationalize the observed conductivity variation based on the bond valence analysis of MD simulated configurations that did not contain P–Cl bonds [23].

A comparative study of LiBr-doped lithium tellurite glasses with LiCl-doped glasses reported that the σ and thermal expansion values are lower, and T_g values are higher for LiBr-doped glasses than for LiCl-doped glasses. These phenomena are attributed to the strength of the Te–O_{ax} bond (ax denotes axial position) and the amount of TeO_2; the extent of weakening of the Te–O_{ax} bond, which brings about the formation of TeO^{2-}, is smaller in the LiBr glasses than in the LiCl glasses [24].

In this work, $(LiBr)_x[(Li_2O)_{0.6}(P_2O_5)_{0.4}]_{(1-x)}$ (where $x=0.1$, 0.15, 0.2) glasses were prepared, characterized by impedance spectroscopy; structures were modelled by MD simulation and analyzed by the bond valence approach to understand the relation between conductivity and the pathways for mobile Li^+ ions, as well as the influence of LiBr doping. The results are compared with our previous findings for $(LiCl)_x[(Li_2O)_{0.6}(P_2O_5)_{0.4}]_{(1-x)}$ ($0.1 \leq x \leq 0.2$) [23].

Sample preparation and properties characterization

$(LiBr)_x[(Li_2O)_{0.6}(P_2O_5)_{0.4}]_{(1-x)}$ glasses ($x=0.1$, 0.15, 0.20) were prepared by conventional melt quenching using $NH_4H_2PO_4$, Li_2CO_3, and LiBr. The mixture of $NH_4H_2PO_4$ and Li_2CO_3 was first heated in a platinum crucible at 300 °C for 1 h, then at 600 °C for 1 h to remove all volatile products, followed by homogenization of the melt at 800 °C for 30 min. LiBr was slowly added to the mixture at 800 °C, while stirring the melt. The melt was kept at 800 °C for 5 min before quenching between two copper plates, which were preheated at 200 °C to avoid shattering of quenched sample. Because LiBr partially evaporates during the preparation, the exact composition of the prepared sample was determined from scanning electron microscopy with the aid of energy dispersive X-ray analysis (EDX). Bromide wt.% obtained from EDX was used to quantify the exact composition for each prepared glass [$x = $ (wt.% of Br/100) (M_{glass}/M_{Br}), M: atomic mass in g/mol]. Table 1 shows a comparison between expected and observed bromide contents in the corresponding glasses. The quenched samples were characterized by X-ray powder diffractometry using Cu K_α radiation (PANalytical X'Pert PRO, equipped with a fast linear X'Celerator detector). XRD patterns in the 2θ range

Table 2 Physical parameters of $(LiBr)_x[(Li_2O)_{0.6}(P_2O_5)_{0.4}]_{(1-x)}$

Nominal composition	T_g/K (±2)	σ_{MD} [σ_{exp}]/Scm^{-1} at 27°C	Experimental density/gcm^{-3}	Number density/Å^{-3}
$(Li_2O)_{0.54}(P_2O_5)_{0.36}(LiBr)_{0.10}$	573	3.53×10^{-7} [3.18×10^{-7}]	2.392(2)	8.23×10^{-2}
$(Li_2O)_{0.51}(P_2O_5)_{0.34}(LiBr)_{0.15}$	552	1.13×10^{-6} [0.98×10^{-6}]	2.421(1)	8.01×10^{-2}
$(Li_2O)_{0.48}(P_2O_5)_{0.32}(LiBr)_{0.20}$	540	2.97×10^{-6} [2.72×10^{-6}]	2.443(1)	7.78×10^{-2}

Fig. 1 L.H.S.: Nyquist plots of $(Li_2O)_{0.54}(P_2O_5)_{0.36}(LiBr)_{0.10}$ glass at different temperatures and equivalent circuit used for fitting. *Red solid line*: fit at $T=$ 300 K. R.H.S.: Arrhenius plots of d.c. conductivities obtained from impedance spectroscopy for different glasses
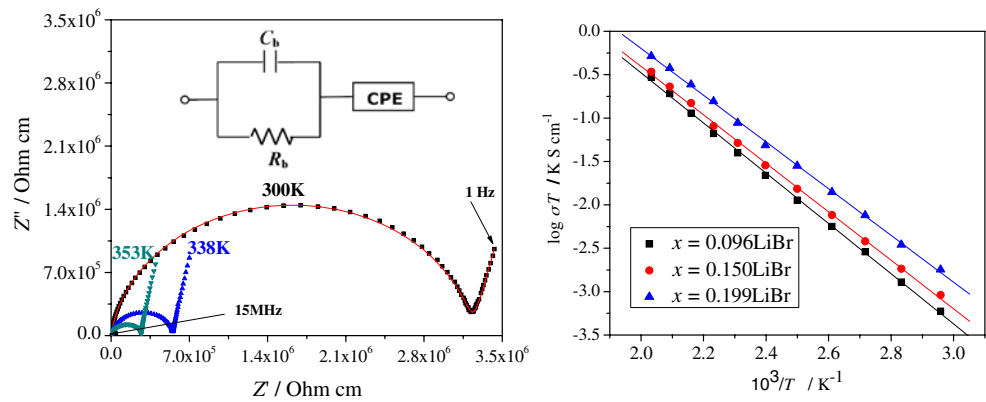
10° to 80° show no sharp Bragg peaks confirming the glassy nature of the samples. Glass densities were measured by Pycnometry; the glass transition temperature, T_g by differential scanning calorimetry (DSC; *TA Instruments 2920 Modulated DSC*) at a heating rate of 10 K/min under constant flow of high purity N_2.

Ionic conductivity measurements at different temperatures were carried out by electrochemical impedance spectroscopy (*Schlumberger Solartron SI 1260*) in the frequency range of 1 Hz to 15 MHz. Commercially available silver paint (ion-blocking electrode) was applied on both sides of the glass sample to achieve a controlled contact area for the ionic conductivity determination. At each temperature, the sample was kept for 10 min for equilibration. The bulk resistance R_b was determined from fitting impedance data to Nyquist plots using an equivalent circuit model. The equivalent circuit consists of C_b, R_b, and CPE, where C_b is the geometric capacitance of the sample between the electrodes, and CPE is the constant phase element due to the polarization distribution at the interface between blocking electrodes and glass.

Constant volume (NVT) MD simulations have been performed on structure models of $(1-x)(0.6Li_2O–0.4P_2O_5)–xLiBr$ glasses (where $x=0.10$, 0.15, 0.20). The volume of the simulation box is derived from our density determi-

nations. Details of the simulations were given elsewhere [23]. Bond valence analysis is applied to the final configuration obtained at 300 K.

Bond valence approach

Empirical relationships between the length $R_{A–X}$ of the bond between cation A and anion X and its bond valence (BV) $s_{A–X} = \exp[(R_0\text{-}R_{A–X})/b_0]$ are widely used to identify plausible equilibrium sites for an atom in a structure as sites where the sum $V(A)$ over all $s_{A–X}$ matches the oxidation state of A [25]. Here, the empirical bond valence parameters R_0 and b_0 quantify the distance between A and X when the individual bond valence is unity, and the softness of the A–X interaction (see tables of BV parameters e.g. in [26, 27]). As we demonstrated recently [26–29], "accessible" sites for an ion A can be identified as sites where the mismatch of $V(A)$ over the $s_{A–X}$ from all adjacent counterions, X remains small. Chemical plausibility of BV mismatch "energy landscapes," $|\Delta V(A)|$, is enhanced by a penalty function, $p_{A–X}$, that discriminates against sites where a matching $V(A)$ is achieved by strongly asymmetric coordination [27, 29]. Coulomb repulsions are considered between mobile and immobile cations only. Isosurfaces of fixed maximum $|\Delta V(A)|$ will

Fig. 2 Ionic conductivities (*left*, $T=27$ °C) and activation energies (*right*) vs. LiX content for $(LiBr)_x[(Li_2O)_{0.6}(P_2O_5)_{0.4}]_{(1-x)}$. *Lines* polynomial fits
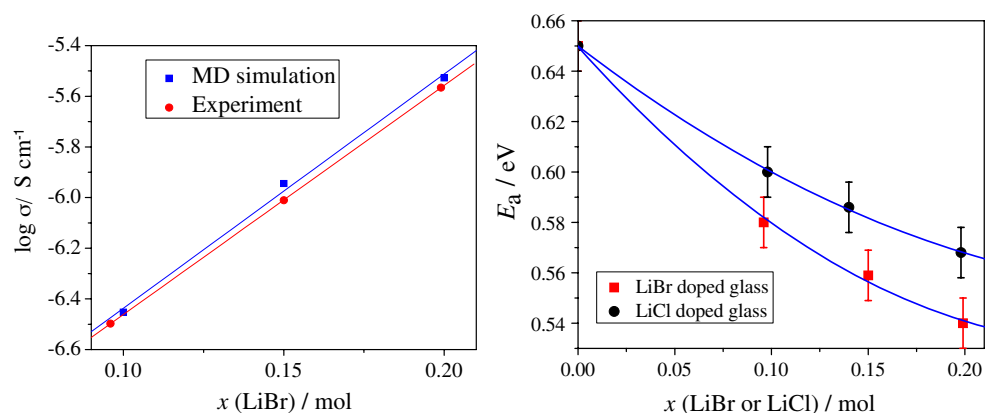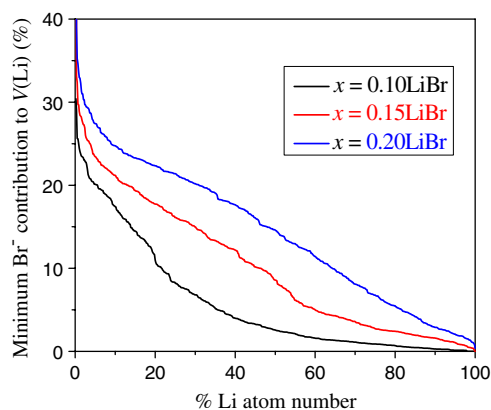
Fig. 3 Distribution of relative contributions of Li–Br bonds to V(Li) in $(LiBr)_x[(Li_2O)_{0.6}(P_2O_5)_{0.4}]_{(1-x)}$ for $x=0.1$ to 0.2

enclose regions that an A ion in the pathway may reach with a certain activation energy, E_a (as discussed more in detail in [29], E_a is proportional to $\Delta V(A)^2$). Regions of low BV mismatch that include both occupied and vacant sites enable local jumps of A. To model pathways, the structure model (here, a snapshot from the MD simulation) is divided into a primitive grid containing ~3 million cubic volume elements with a size of ca. $(0.2 \text{ Å})^3$, and a volume element is considered to belong to the conduction pathway if $|\Delta V(A)|$ is below a fixed threshold value or if the sign of $\Delta V(A)$ alters within the volume element. These pathway clusters (of accessible volume elements) contribute to d.c. conductivity if they percolate through the structure model. The volume fraction, F, of the percolating pathways is a suitable measure of E_a and thereby (in the case of glasses) also of the room temperature conductivity [26–29]. The remaining restricted pathway clusters are considered to contribute only to a.c. conductivity.
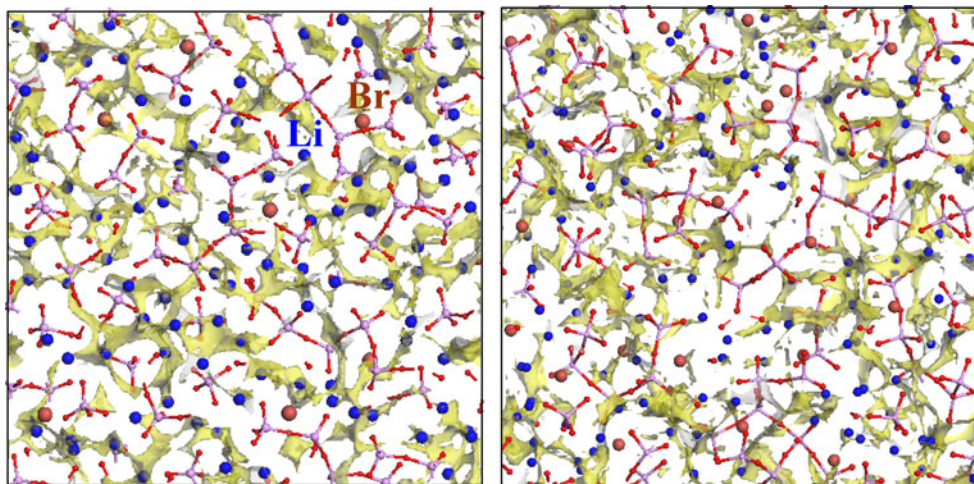
Results and discussions

While mass densities increase, number density decrease with rising LiBr content (Table 2), indicating that the glass network becomes more open, which together with the higher polarizability of Br^- decreases T_g (see Table 2) and increases the Li^+ ion mobility. The decrease in T_g with the increase of LiBr content indicates the glass matrix becomes less rigid with the LiBr addition, in line with the literature reports for LiCl-doped glasses [15, 23]. It may still be noted that T_g values are ca. 5 K higher for the LiBr-doped glasses than for LiCl-doped glasses [23]. Complex impedance spectra of the glasses were measured over the temperature range from 27 to 219 °C. Figure 1 shows that impedance data can be fitted by the simple equivalent circuit and that the bulk conductivity determined from these fits follows Arrhenius-type temperature dependence. The activation energy (E_a) decreases from 0.58 eV for $x=0.1$ to 0.54 eV for $x=0.2$. As seen in Fig. 2, MD simulation quantitatively reproduces the experimental values within experimental uncertainties. For the same value of x and Li_2O/P_2O_5 ratio, LiBr-doped glasses exhibit lower E_a values than LiCl-doped ones. The drop in E_a as a function of x can be approximated as $E_a = 0.64 - C_1 x + C_2 x^2$ with $C_1=0.85$, $C_2=1.54$ for LiBr- and $C_1=0.58$, $C_2=0.88$ for LiCl-doped glasses.

Final equilibrated MD configurations of these glasses were used for bond valence (BV) analysis. It was confirmed that the percentage of bridging and non-bridging oxygen (23% and 77%, respectively) did not vary with the addition of LiBr. The BV approach can also be employed to clarify whether the Li^+ ions form LiBr clusters in the investigated glass structures. This hypothesis can be ruled out for the system under study: the distribution of relative contributions of Li–Br bonds to the lithium BV sums in these glasses (Fig. 3) demonstrates that <2% of the Li atoms are

Fig. 4 Slices through the Lithium migration pathway network visualized as isosurfaces of constant lithium bond valence sum mismatch $|\Delta V(Li)|$ for the LiBr contents $x=0.10$ (l.h.s.) and $x=0.20$ (r.h.s.) at 300 K superimposed on the respective glass structure model

Fig. 5 Variation of Li$^+$ ion pathway volume fraction with experimental room temperature ionic conductivity (l.h.s.) and activation energy (r.h.s.). *Solid symbols* refer to data from RMC models [23]; *open symbols* refer to MD simulated of $(LiX)_x[(Li_2O)_{0.6}(P_2O_5)_{0.4}]_{(1-x)}$ glass structures: *triangles* LiX= LiBr (this work), *circles* LiX= LiCl ($0.1 \leq x \leq 0.25$) [20]
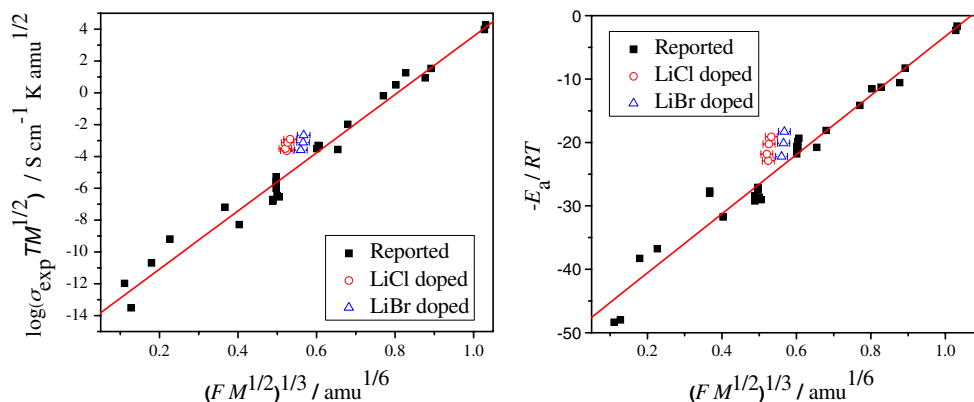
bonded predominantly by bromide ions, and none of the Li atoms is coordinated exclusively by Br$^-$. More than 95% oxide bonding occurs for 18% (x=0.2, O/Br ratio 10:1) to 64% (x=0.1, O/Br ratio 23:1) of the Li atoms. Thus, any Li$^+$ ion transport pathway has to run along sites with mixed oxide/halide or exclusive oxide coordination. Figure 3 shows the local environment of the Li$^+$ ion sites located in the conduction pathways of glasses under present investigation. Figure 4 visualizes the conduction pathways in two of the investigated glasses (modeled as isosurfaces of constant Li bond valence sum mismatch) along with the glass network (with PO$_4$ terahedra and Li, Br atoms) at 300 K. Although the pathways appear to be discontinuous ribbons in the displayed slices, nearly all the displayed pathway sections belong to the percolating pathway cluster. The density of pathways slightly increases with increasing Br$^-$ content from x=0.10 to 0.20 (see Fig. 4; the volume fraction of percolating pathways (F) increases from 6.67 (5)% to 6.93(5)%), in line with the slight increase of ionic conductivity in these glasses. The volume fraction F in LiBr-doped glasses is higher than that of LiCl-doped glasses correspondingly, which is from 5.4% to 5.8% [23]. This contributes to higher conductivity of LiBr-doped glasses when compared to LiCl-doped glasses for the same value of LiX doping (X=Cl$^-$, Br$^-$).

Using a bond valence mismatch value of $|\Delta V(A)|$ of 0.1 valence units (to allow for a comparison with existing reference data for a wide range of oxide glasses), we could also show that the room temperature ionic conductivity in these glasses can be semiquantitatively predicted from the structure model. Figure 5 relates the volume fraction of the percolating ion conduction pathways in the investigated glasses to the experimentally observed absolute values of the ionic conductivity and activation energy (E_a). Results of the present MD study are compared with the previously reported Reverse Monte Carlo (RMC) values and LiCl-doped glasses. As seen from Fig. 5, the increase in F (1) when increasing the dopant concentration x or (2) when

replacing Cl$^-$ by the same amount of Br$^-$ leads to an increase in the ionic conductivity and a corresponding decrease in the activation energy.

Using the concept of mass-radius dimension [29], we can further investigate details of the pathway structure. As seen from Fig. 6, the minimum value of local pathway dimension increases with the LiBr content. This minimum value of local dimension may be largely thought of as characterizing the width of the Li ion transport pathway at the bottleneck of elementary transport steps. Thus, the increase of the local pathway dimension as a result of doping by the more polarizable Br$^-$ ion indicates that channels accessible for Li$^+$ ion movement are widened by the doping. This contributes to the decrease of activation energy and increase of ionic conductivity and with rising LiBr content.
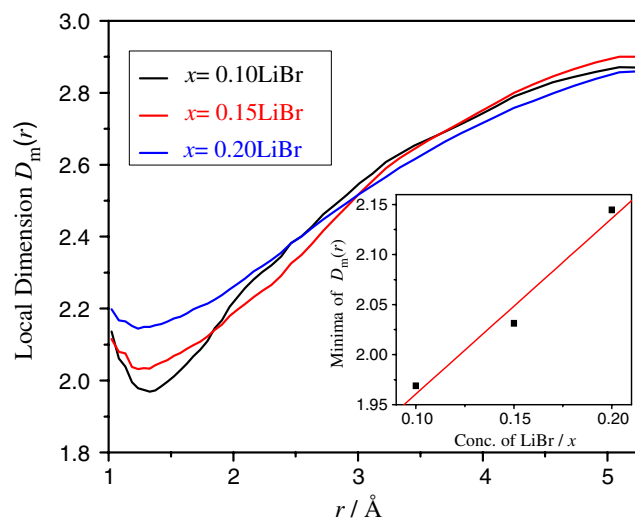
Fig. 6 The local Li$^+$ ion transport pathway dimension, $D_m(r)$ *vs.* radius (r) for $(LiBr)_x[(Li_2O)_{0.6}(P_2O_5)_{0.4}]_{(1-x)}$ glasses. *Inside graph* indicates the variation of local dimension minima with respect to LiBr variation

Summary

Optimized potential parameters reproduce the reported bond lengths and coordination. Moreover, experimental and simulated values of the ionic conductivity are in good agreement. The effect of LiBr addition on the pathways for the mobility of Li$^+$ ions is quantified for the phosphate glasses xLiBr-$(1-x)(0.6Li_2O-0.4P_2O_5)$. Volume fraction for Li ion transport pathway and experimental conductivities accordingly exhibit an unusually small effect of halide doping. For the investigated compositions, ion transport cannot be related to the (previously reported) LiBr aggregates as such aggregates do not exist—at least in the simulated structures. Nearly all Li have mixed oxide bromide coordination. The minimum value of the local pathway dimension increases with the LiBr content. The higher minimum local dimension means that Li ion transport pathway is more open, i.e., channels for Li$^+$ ion hopping become wider. Replacement of LiCl by LiBr causes lower E_a, higher ionic conductivity, and T_g.

References

1. Malugani JP, Robert G (1979) Mater Res Bull 14:1075
2. Brow RK (2000) J Non-Cryst Solids 263&264:1
3. Hoppe U, Walter G, Kranold R, Stachel D (2000) J Non-Cryst Solids 263&264:29
4. Adams S, Swenson J (2002) PCCP 4:3179
5. Karthikeyan A, Vinatier P, Levasseur A, Rao KJ (1999) J Phys Chem B 103:6185
6. Liang J-J, Cygan RT, Alam TM (2000) J Non-Cryst Solids 263&264:167
7. Alam TM, Liang J-J, Cygan RT (2000) PCCP 2:4427
8. Sistla RK, Seshasayee M (2004) J Non-Cryst Solids 349:22
9. Adams S (2006) Bull Mater Sci 29(6):1
10. Vogel M (2003) Phys Rev B 68:184301
11. Tatsumisago M, Kowada Y, Minami T (1988) Phys Chem Glasses 29(2):63
12. Doreau M, Abou El Anouar A, Robert G (1980) Mater Res Bull 15:285
13. Horiuchi M, Sei T, Tsuchiya T (1994) J Non-Cryst Solids 177:236
14. Muruganandam K, Seshasayee M, Patnaik S (1996) Solid State Ionics 89:313
15. Prasada Rao R, Seshasayee M (2004) Solid State Commun 131(8):537
16. Tuller HL, Button DP, Uhlmann DR (1980) J Non-Cryst Solids 40:93
17. Irion M, Couzi M, Levasseur A, Reau JM, Brethous JC (1980) J Solid State Chem 31:285
18. Hall A, Adams S, Swenson J (2006) Phys Rev B 74:174205
19. Tanaka K, Yoko T, Yamada H, Kamiya K (1988) J Non-Cryst Solids 103:250
20. Iwadate Y, Kenmotsu H, Hattori T (2000) J Alloys Compd 305:130
21. Ogiwara Y, Echigo K, Hayana M (2006) J Non-Cryst Solids 352:5192
22. Muller W, Kruschke D, Torge M, Grimmer A (1987) Solid State Ionics 23:53
23. Prasada Rao R, Tho TD, Adams S (2009) J Power Sources 189:385
24. Tanaka K, Yoko T, Kamiya K, Yamada H, Sakka S (1991) J Non-Cryst Solids 135:211
25. Brown ID (2002) The chemical bond in inorganic chemistry: the bond valence model. Oxford University Press, New York
26. Adams S (2001) Acta Crystallogr Sect B Struct Sci 57:278
27. softBV (2005) BV database for Cations. Accessed at http://www.softBV.net; accessed on 20 Jun 2009
28. Adams S, Swenson J (2004) Solid State Ionics 175:665
29. Adams S, Prasada Rao R (2009) PCCP 11:3210